JOURNAL OF SOLID STATE CHEMISTRY 71, 12–18 (1987)

Structure of $PbSb_2O_6$ and Its Relationship to the Crystal Chemistry of PbO_2 in Antimonial Lead-Acid Batteries

RODERICK J. HILL

CSIRO Division of Mineral Chemistry, P.O. Box 124, Port Melbourne, Victoria 3207, Australia

Received September 19, 1986

The crystal structure of $PbSb_2O_6$, space group $P\bar{3}1m$, $a = 5.3006(1)$, $c = 5.3792(1)$ Å, $V = 130.89(2)$ Å^3, $Z = 1$, $D_x = 6.936$ g cm^{-3}, has been refined at 295 K by Rietveld analysis of step-scan neutron powder diffraction data ($\lambda = 1.500$ Å, $\mu = 0.179$ cm^{-1}): $R_{wp} = 0.0614$ for 2898 step intensities, $R_B = 0.0141$ for 150 reflections. The structure consists of gibbsitelike sheets of edge-sharing SbO_6 octahedra oriented perpendicular to the c-axis. These sheets alternate with layers of isolated PbO_6 octahedra positioned above and below the vacant sites in the adjacent $(Sb_2O_6)^{2-}$ layers. The SbO_6 octahedra have symmetry 32 and a bond length of 1.9904(4) Å; the PbO_6 octahedra have symmetry $\bar{3}m$ and a bond length of 2.5633(6) Å. The properties of this structure and its relationship to the polymorphs of PbO_2 provide possible explanations for the well-known beneficial effect of antimony on the cycle life of lead-acid batteries.

Introduction

The compound $PbSb_2O_6$ is of considerable importance since it is the type structure for a number of binary antimonates and arsenates (*1, 2*), as well as rare earth ternary tellurates (*3*). However, the discussion here focuses primarily on the possible role of $PbSb_2O_6$ in the operation of positive plates in antimonial lead-acid batteries; the analysis forms part of a continuing study of the crystal and electrochemical properties of phases in the Pb/Sb/O/H system (*4–7*).

The charged, positive electrode of a "flat plate" lead-acid battery consists of a porous, polycrystalline aggregate of PbO_2 residing on a lead-alloy grid (*8, 9*). When batteries are required to have an extensive cycling capability (e.g., in electric-vehicle applications), the lead grid usually contains between 3 and 6 wt% antimony in order to improve its castability, corrosion resistance, and mechanical strength. However, the requirement for antimony is not limited to improving the properties of the grid. There is evidence (*10–13*) that antimony leached from the positive plate grid during battery operation improves the cycle life and capacity performance of the positive-plate material by promoting the growth of the orthorhombic alpha polymorph of PbO_2 (as opposed to the tetragonal beta form), by modifying the size and morphology of the PbO_2 crystals, and by improving the adhesion between the PbO_2 particles and the grid.

The mechanism by which antimony affects PbO_2 crystal size and morphology has yet to be clarified, but it appears to act simultaneously as both a nucleating agent and a growth inhibitor, either by direct substitution of Sb^{5+} ions for Pb^{4+} ions and/or

0022-4596/87 $3.00

interstitials/vacancies in the structure of PbO_2 or by preferential adsorption of a soluble antimony species onto the growing crystal faces (*12, 14–17*). The action of antimony in promoting the formation of α-PbO_2 relative to β-PbO_2 during battery plate operation has been associated both with the greater extent of incorporation of antimony in the α-PbO_2 polymorph (*15*) and with the formation of the compound $PbSb_2O_6$ (*18, 19*).

The structure of $PbSb_2O_6$ was determined by Magneli (*1*) using single-crystal X-ray diffraction photographic data. The lead and antimony atoms were assigned to special positions in space group $P312$, and the oxygen atom coordinates were determined from crystal-chemical considerations and adjusted by trial-and-error methods. A refinement of this structure using neutron data is desirable, not only because of the uncertainty associated with the X-ray-determined oxygen atom coordinates, but also because the assigned space group appears to have unnecessarily low symmetry for the structure proposed.

Experimental

A pure, white, powder sample of $PbSb_2O_6$ was prepared from stoichiometric amounts of orthorhombic PbO and cubic Sb_2O_3 by heating the mixture in a silica dish in air for 6 hr at 1125 K, grinding, and reheating for 100 hr at 1225 K. Neutron diffraction data were collected at 295 K on the high-resolution, fixed-wavelength, eight-counter diffractometer (HRPD) attached to the Australian Atomic Energy Commission research reactor HIFAR at Lucas Heights, New South Wales. This instrument (in an earlier single-counter configuration) has been described in detail elsewhere (*20*). The sample was contained in a 16 × 50-mm spinning vanadium can and data were recorded under monitor control at intervals of 0.05° between 15 and 159.85 2θ.[1] For the wavelength 1.500 Å, this range of diffraction angles contains 150 unique Bragg reflections.

Least-squares structure refinements were performed with a modified Rietveld analysis program (*5, 21*) incorporating a Voigt peak shape function, a correction for sample absorption in the neutron beam, an asymmetry correction involving a sum of five Voigtian peaks, and a background function defined by a four-parameter polynomial in $2\theta^n$, where n has values between 0 and 3. The calculated peak intensity was distributed over four peak full-widths at half-maximum on either side of the peak center. The function minimized was $w_i (Y_{io} - Y_{ic})^2$, where Y_{io} and Y_{ic} are the observed and calculated intensities at each step i in the pattern and $w_i = 1/Y_{io}$. The refinement was terminated when the parameter shifts were less than 10% of their associated esd's. The scattering lengths used for Pb, Sb, and O were 9.401, 5.640, and 5.805 fm, respectively.

The refinement was initiated in space group $P312$ with the single Pb and two Sb atoms in special positions 1*a*, 1*d*, and 1*f*, respectively, and the O atom in general position 6*l* with coordinates (0.375, 0.0, 0.292), as determined by Magneli (*1*). Although the general arrangement of atoms in the unit cell was found to be correct for this model (as indicated by reasonable values for all agreement indices), convergence

[1] See NAPS document No. 04518 for 6 pages of step-scan diffraction data deposited as supplementary material. Order from ASIS/NAPS, Microfiche Publications, P.O. Box 3513, Grand Central Station, New York, NY 10163. Remit in advance $4.00 for microfiche copy or for photocopy, $7.65 up to 20 pages plus $0.30 for each additional page. All orders must be prepaid. Institutions and Organizations may order by purchase order. However, there is a billing and handling charge for this service of $15. Foreign orders add $4.50 for postage and handling, for the first 20 pages, and $1.00 for additional 10 pages of materials, $1.50 for postage of any microfiche orders.

could not be achieved when the O atom coordinates were released. This refinement instability added to suspicions about the structural model that had already been aroused by the presence of two unit-multiplicity Sb atom sites and a zero value for the variable y-coordinate of O; both of these factors suggested that space group $P312$ had unnecessarily low symmetry.

Other space group possibilities were therefore examined which left the atomic arrangement intact but provided a twofold special position for Sb and a special position of the kind (x, 0, z) for O. These three conditions are met simultaneously only by space group $P\bar{3}1m$. A full-matrix, isotropic thermal parameter refinement (14 profile and 5 structural parameters) was therefore continued in $P\bar{3}1m$ and produced rapid convergence to R_{wp} and R_B values of 0.0653 and 0.0244, respectively. Refinements in alternative space groups satisfying only one or two of the above conditions (e.g., space group $P\bar{3}$) produced either unstable refinements or worse fits to the data.

Application of anisotropic thermal vibration ellipsoids to all three atoms in $P\bar{3}1m$ gave further reductions in the agreement indices to the values $R_{wp} = 0.0614$ and $R_B = 0.0141$. These improvements, together with a decrease in the goodness-of-fit index from 1.882 to 1.665, are taken as an indication that the conversion to anisotropic ellipsoids is warranted. It is noted that the shape of the O atom ellipsoid provides no evidence for a significant displacement of this atom from its $y = 0$ position in space group $P\bar{3}1m$. A summary of the refined structural parameters is given in Table I, and the corresponding observed, calculated, and difference diffraction profiles are presented in Fig. 1.

Discussion

Crystal Structure

The refinement results confirm the general atomic arrangement proposed earlier (*1*), but place the atoms under the symmetry constraints of space group $P\bar{3}1m$ rather than $P312$. The isostructural AB_2O_6 antimonates and arsenates (*1*) are also likely to possess this higher symmetry. However, the corresponding ternary tellurates (*3*), if ordered, require a separation of the two B cations into distinct sites and they may therefore retain the symmetry $P312$.

The $PbSb_2O_6$ structure is based on a hexagonal array of oxygen atoms with alternate (001) layers of octahedral interstices that are two-thirds filled by antimony atoms and one-third filled by lead atoms, respectively (Fig. 2). The antimony sheets have an overall composition $(Sb_2O_6)^{2-}$ and consist of gibbsite or honeycomblike rings of edge-

TABLE I

FRACTIONAL ATOMIC COORDINATES AND THERMAL VIBRATION COEFFICIENTS (Å^2)

	x	y	z	β_{11}[a]	β_{22}	β_{33}	β_{13}	B_{eq}[b]
Pb	0	0	0	93(3)[c]	—	82(4)	—	0.84(2)
Sb	$\frac{1}{3}$	$\frac{2}{3}$	$\frac{1}{2}$	36(3)	—	72(4)	—	0.48(2)
O	0.37952(11)	0	0.29531(13)	85(2)	51(3)	76(3)	−24(2)	0.71(1)

[a] Anisotropic thermal vibration coefficients $\times 10^4$.

[b] B_{eq} is defined as $8\pi^2$ (mean-square radial displacement)/3.

[c] Parenthesized figures here and in Table II represent the esd in terms of the least significant figure to the left.

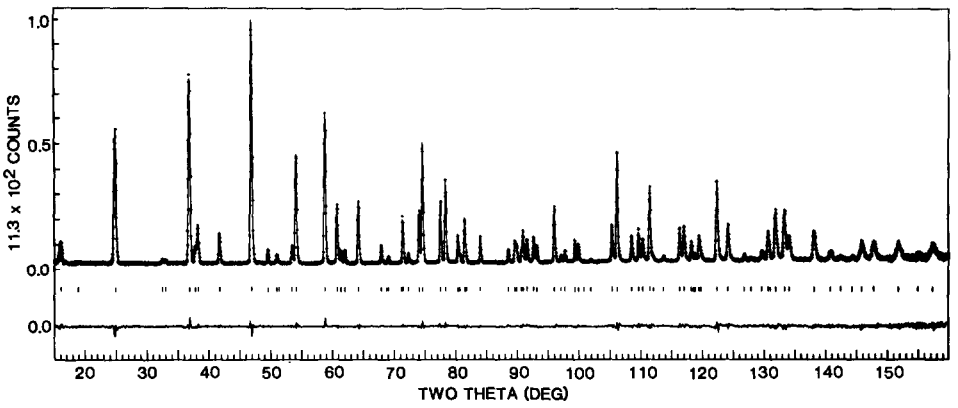

FIG. 1. Observed, calculated, and difference neutron powder diffraction profiles for $PbSb_2O_6$ (1.5 Å). The observed data are indicated by plus signs and the calculated profile is the continuous line in the same field. The short vertical lines below the profiles represent the positions of all possible Bragg reflections, and the bottom curve is the difference between the observed and calculated intensity at each step.

sharing SbO_6 octahedra with symmetry 32 and an Sb–O bond length of 1.9904(4) Å (Table II). The lead atoms are located in isolated octahedral sites with symmetry $\bar{3}m$ and bond length 2.5633(6) Å, positioned above and below the vacant sites (i.e., the centers of the rings) in the antimony layers.

The segregation of the two types of cation into alternate octahedral layers of the AB_2O_6 structure allows a wide range of A cations to be accommodated into the structure (*1*). Figure 3 is a plot of the variation in unit cell dimensions (with values taken from Ref. (*1*)) as a function of the ionic radius (*22*) of the A cation for several antimonates and arsenates with this structure type. The a-axis (in the plane of the octahedron sheets) for both series changes only

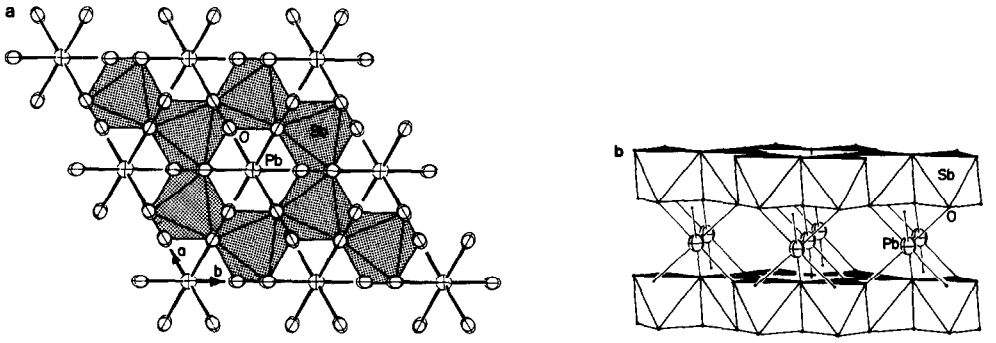

FIG. 2. Diagram of four unit cells of the $PbSb_2O_6$ structure viewed (a) down the c-axis and (b) approximately along the [110] direction. In (a) the Sb atoms (not shown) are located at the center of each shaded, opaque octahedron of O atoms. The Pb atoms are located directly above and below the vacant sites in this layer; only the set of Pb atoms below the plane is shown in (a), connected to their coordination sphere of O atoms by conical bonds. In (b) the SbO_6 octahedra are again opaque, but only the top surfaces are shaded, and the O atoms are represented as dots for the sake of clarity. The interlayer Pb–O bonds are represented by lines. Thermal ellipsoids for all atoms correspond to 99% probability surfaces.

TABLE II

INTERATOMIC DISTANCES (Å) AND ANGLES (°)[a]

Pb–O	2.5633(6) ×6	O . . . O	3.484(1)	85.64(2) ×6
			3.760(1)	94.36(2) ×6
			—	180.0 ×3
Sb–O	1.9904(4) ×6	O . . . O	2.546(1)	79.51(3) ×3
			2.872(1)	92.35(2) ×6
			2.983(1)	97.06(3) ×3
			—	167.77(3) ×3

[a] Calculated assuming no error in the neutron wavelength.

slightly as a function of A cation radius, in spite of the fact that the cation sizes differ by as much as 50%. This occurs because the AO_6 octahedra are isolated from each other (Fig. 2), leaving the layers of edge-sharing BO_6 octahedra to dictate the dimension in the (001) plane. On the other hand, the c-axis (perpendicular to the octahedron sheets) increases substantially in both series as the radius of the A cation increases (Fig. 3). For example, the c/a axial ratio decreases by almost 20% when Cd is substituted for Ba in the antimonate series.

The minimum radius of the A cation accommodated in the antimonates is about 0.95 Å (Cd^{2+}). For smaller A cations (e.g., Mn^{2+}), their segregation into separate layers (from the B cations) is not necessary and the favored ($MnSb_2O_6$) structure can be of the columbite (*23*), trirutile (*24*), or other (*25*) type. For the arsenates, the minimum A cation radius is smaller (i.e., ≈0.7 Å for Ni^{2+}) since the dimensions of the BO_6 octahedra are smaller. Indeed, the upper and lower limits for the value of the $A^{2+}:B^{5+}$ radius ratio are approximately the same for both the antimonates and the arsenates, namely, 2.3 and 1.6, and 2.6 and 1.5, respectively.

Effects of $PbSb_2O_6$ on Battery Operation

Swets (*18*) attempted to explain the higher α-PbO_2 contents (relative to β-PbO_2) observed in antimonial lead-acid battery plates by analyzing the structures of $PbSb_2O_6$ and both polymorphs of PbO_2 in terms of a possible epitaxial relationship that would permit nucleation and/or passivation of the dioxide surfaces. Unfortunately, this earlier discussion was relatively unconvincing because it focused on differences in the connectivity between the PbO_6 octahedra in α-PbO_2 and β-PbO_2, namely, zigzag and straight chains, respectively (*26*). Indeed, considerations of the likelihood of epitaxial relationships between structures should concentrate on the geometrical fit between the constituent layers of close-packed anions rather than on the details of the cation-ordering pattern.

With this in mind, the hexagonally close-packed layers of anions in $PbSb_2O_6$ and the two polymorphs of PbO_2 are displayed schematically in Fig. 4, along with the corresponding cation distributions and orthogonal anion repeat distances in the close-packed planes (taken from Ref. (*26*)). The figure clearly demonstrates that the repeat distances in $PbSb_2O_6$ (3.06 and 5.31 Å) are

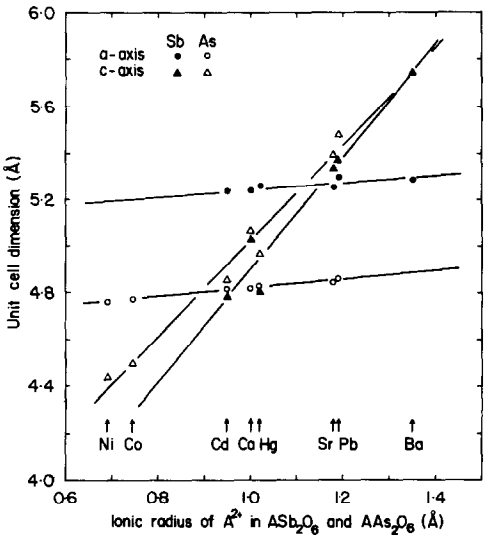

FIG. 3. Unit cell dimensions a and c of the compounds ASb_2O_6 and AAs_2O_6 as a function of the ionic radius of the divalent cation A. With the exception of $PbSb_2O_6$, all cell dimensions have been taken from Ref. (*1*). The lines represent the least-squares regression relationship between the quantities plotted.

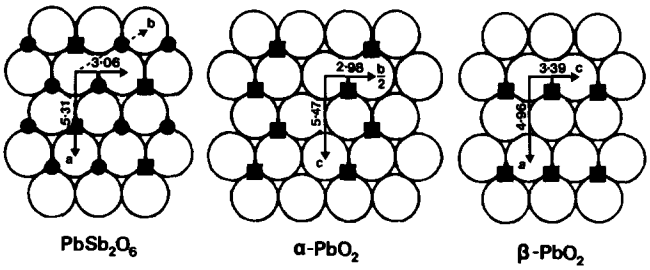

FIG. 4. Schematic representation of the hexagonal close-packed layers of O atoms (large open circles) and cation ordering patterns (solid circles = Sb; solid squares = Pb) in the crystal structures of $PbSb_2O_6$, α-PbO_2, and β-PbO_2. The repeat distances (Å) for the O-atom hexagonal arrays were determined from the corresponding unit cell dimensions (present study and Ref. (*26*)).

very similar to those in α-PbO_2 (2.98 and 5.47 Å), but are quite different from those in β-PbO_2 (3.39 and 4.96 Å). This suggests that an epitaxial relationship between $PbSb_2O_6$ and α-PbO_2 is quite feasible, whereas a similar relationship with β-PbO_2 is most unlikely. Thus, the presence of Sb (as $PbSb_2O_6$) in the positive plates of lead-acid batteries can be expected, as observed, to promote the growth of α-PbO_2 (and vice versa) during both the formation and charging stages of battery operation.

The greater adherence of the corrosion layer to the lead-acid battery grid when an antimonial alloy is used instead of pure lead has been attributed to a reduced incidence of stress-cracking in the corrosion layer (*14*). The reduced cracking has, in turn, been related to the additional space resulting from the preferential leaching of antimony-rich regions from the grid (*27*), and to the reduced hardness of antimonial oxide (*28*). The hardness of $PbSb_2O_6$ should indeed be lower than that of PbO_2 since the antimonate contains relatively weak, long Pb^{2+}–O bonds with a nominal (formal) strength (*29*) of only 0.33 valence units (v.u.), localized into layers. While the short Sb^{5+}–O bonds in $PbSb_2O_6$ are stronger than the Pb^{4+} bonds in PbO_2 (viz., 0.83 vs 0.67 v.u., respectively), the marked anisotropy of bond strength in $PbSb_2O_6$ may be expected to provide the opportunity for micro-slippage/cleavage of the layers over each other under the stresses of corrosion-product transformations during battery charge and discharge, thus preventing the formation of large cracks that ultimately lead to loss of adherence of the oxide to the grid (*14*).

Alternative Grid-Alloy/Dopant Elements

A large number of dopant elements have been tested, at one time or another, in an effort to meet the requirements of lead-acid battery grid alloys. Not the least of these have been the elements adjacent to antimony (and lead) in periods 4 to 6 and groups IVA to VIA in the Periodic Table, namely, As, Sn, Se, Te, and Bi. The effects of these elements on the properties of the alloys are well documented (see, for example, Ref. (*30*)), but their influence on the mechanism of grid corrosion and (as oxides) on the performance of the positive-plate material during battery charge/discharge has not been elucidated.

The elements adjacent to Pb have many crystal-chemical properties in common with Sb and often form dimorphous, or closely related, structures when combined with oxygen. Prime examples of this crystal-chemical similarity include the formation of isostructural binary antimonates and arsenates (*1*) and the presence of equivalent substructure building units in the structures of tetragonal PbO, orthorhombic PbO_2, $Pb_3O_2(OH)_2$, Sb_2O_3, and the "inter-

mediate" lead oxides PbO_x (*4*). In addition, at least one of the elements (i.e., Sn) has been observed to form basic sulfates and oxide/hydroxides analogous to those of lead (*31, 32*).

Whether or not these elements will provide the benefits of antimony in terms of greater adhesion of the positive-plate material to the grid, as well as improved cycling performance, without the detrimental side effects (e.g., self-discharge and electrolyte loss), remains to be determined, but the crystal-chemistry of the system suggests that such prospects are good.

Acknowledgments

The author is grateful to Drs. I. E. Grey and D. A. J. Rand for their careful reviews of the manuscript. The work was undertaken with the financial assistance of the Australian Associated Smelters Pty. Ltd.

References

1. A. MAGNELI, *Ark. Kemi, Mineral. Geol. B* **15,** 1 (1941).
2. J. B. TAYLOR AND R. D. HEYDING, *Canad. J. Chem.* **36,** 597 (1958).
3. H. M. KASPER, *Mater. Res. Bull.* **4,** 33 (1969).
4. R. J. HILL, *Acta Crystallogr., Sect. C* **41,** 998 (1985).
5. R. J. HILL, *Acta Crystallogr., Sect. C* **41,** 1281 (1985).
6. R. J. HILL AND I. C. MADSEN, *J. Electrochem. Soc.* **131,** 1486 (1984).
7. R. J. HILL, A. M. JESSEL, AND I. C. MADSEN, *in* "Proceedings, Symposium on Advances in Lead-Acid Batteries" (K. R. Bullock and D. Pavlov, Eds.), Vol. 84-14, p. 59, Electrochemical Society, Pennington, NJ (1984).
8. J. BURBANK, A. C. SIMON, AND E. WILLINHGANZ, *in* "Advances in Electrochemistry and Electrochemical Engineering" (P. Delahay and C. W. Tobias, Eds.), Vol. 8, p. 157, Wiley, New York (1970).
9. J. PERKINS, *Mater. Sci. Eng.* **28,** 167 (1977).
10. J. BURBANK, *J. Electrochem. Soc.* **111,** 1112 (1964).
11. D. KORDES, *Chem. Ing. Techn.* **38,** 638 (1966).
12. E. J. RITCHIE AND J. BURBANK, *J. Electrochem. Soc.* **117,** 299 (1970).
13. J. L. DAWSON, M. I. GILLIBRAND, AND J. WILKINSON, "Power Sources 3" (D. H. Collins, Ed.), p. 1, Oriel Press, Newcastle upon Tyne, UK (1970).
14. B. K. MAHATO, *J. Electrochem. Soc.* **126,** 365 (1979).
15. F. CALDARA, A. DELMASTRO, G. FRACCHIA, AND M. MAJA, *J. Electrochem. Soc.* **127,** 1869 (1980).
16. H. NGUYEN CONG, A. EJJENNE, J. BRENET, AND P. FABER, *J. Appl. Electrochem.* **11,** 373 (1981).
17. A. BOGGIO, M. MAJA, AND N. PENAZZI, *J. Power Sources* **9,** 221 (1983).
18. D. E. SWETS, *J. Electrochem. Soc.* **120,** 925 (1973).
19. F. ARIFUKU, H. YONEYAMA, AND H. TAMURA, *J. Appl. Electrochem.* **11,** 357 (1981).
20. C. J. HOWARD, C. J. BALL, R. L. DAVIS, AND M. M. ELCOMBE, *Austral. J. Phys.* **36,** 507 (1983).
21. R. J. HILL AND C. J. HOWARD, "A Computer Program for Rietveld Analysis of Fixed Wavelength X-Ray and Neutron Powder Diffraction Patterns," Report No. M112, Australian Atomic Energy Commission, Lucas Heights Research Laboratories, PMB, Sutherland, New South Wales, Australia (1986).
22. R. D. SHANNON, *Acta Crystallogr., Sect. A* **32,** 751 (1976).
23. K. BRANDT, *Ark. Kemi, Mineral. Geol. A* **17,** 1 (1943).
24. F. SALA AND F. TRIFIRO, *J. Catal.* **41,** 1 (1976).
25. H. G. SCOTT, *J. Solid State Chem.* **66,** 171 (1987).
26. R. J. HILL, *Mater. Res. Bull.* **17,** 769 (1982).
27. A. C. SIMON, *J. Electrochem. Soc.* **114,** 1 (1967).
28. S. HATTORI, M. YAMAURA, M. KINO, M. YAMANE, H. NAKASHIMA, J. YAMASHITA, AND J. NAKAYAMA, Report No. 5, ILZRO Project No. LE-276, International Lead Zinc Research Organization, Inc., 292 Madison Ave., New York (1980).
29. L. PAULING, "The Nature of the Chemical Bond," 3rd ed., p. 548, Cornell Univ. Press, Ithaca, NY (1960).
30. D. PAVLOV, "Studies in Electrical and Electronic Engineering 11. Power Sources for Electric Vehicles" (B. D. McNicol and D. A. J. Rand, Eds.), Chap. 5.1, Elsevier, Amsterdam (1984).
31. R. A. HOWIE AND W. MOSER, *Nature (London)* **219,** 372 (1968).
32. S. GRIMVALL, *Acta Chem. Scand.* **27,** 1447 (1973).